In vivo and in vitro measurements of pulmonary arterial stiffness: A brief review

Lian Tian and Naomi C. Chesler

Department of Biomedical Engineering, University of Wisconsin-Madison, Madison, Wisconsin, USA

ABSTRACT

During the progression of pulmonary hypertension (PH), proximal pulmonary arteries (PAs) undergo remodeling such that they become thicker and the elastic modulus increases. Both of these changes increase the vascular stiffness. The increase in pulmonary vascular stiffness contributes to increased right ventricular (RV) afterload, which causes RV hypertrophy and eventually failure. Studies have found that proximal PA stiffness or its inverse, compliance, is strongly related to morbidity and mortality in patients with PH. Therefore, accurate in vivo measurement of PA stiffness is useful for prognoses in patients with PH. It is also important to understand the structural changes in PAs that occur with PH that are responsible for stiffening. Here, we briefly review the most common parameters used to quantify stiffness and in vivo and in vitro methods for measuring PA stiffness in human and animal models. For in vivo approaches, we review invasive and noninvasive approaches that are based on measurements of pressure and inner or outer diameter or cross-sectional area. For in vitro techniques, we review several different testing methods that mimic one, two or several aspects of physiological loading (e.g., uniaxial and biaxial testing, dynamic inflation-force testing). Many in vivo and in vitro measurement methods exist in the literature, and it is important to carefully choose an appropriate method to measure PA stiffness accurately. Therefore, advantages and disadvantages of each approach are discussed.

Key Words: pulmonary arterial stiffness, pulmonary artery, pulmonary hypertension

Pulmonary hypertension (PH) is characterized by chronically high blood pressure in the pulmonary circulation, including the pulmonary arteries (PAs), capillaries and veins. PH can occur due to left heart disease, lung disease, hypoxia, recurrent pulmonary embolism, drugs and toxins, or other unknown causes.[1] Regardless of the cause, PH is associated with changes in proximal and distal PAs, which decrease pulmonary vascular compliance and increase pulmonary vascular resistance, respectively. These pulmonary vascular changes increase right ventricular (RV) afterload, causing RV hypertrophy and eventually RV failure.[2-8]

Currently, diagnosis of PH is based on an elevated pulmonary vascular resistance (PVR), which is the viscous hydraulic opposition to the mean blood flow. However, PVR can only provide limited insight into the state of the pulmonary vasculature since it does not consider the pulsatile components of blood flow.[9,10] These pulsatile components of blood flow can be accessed via the pulmonary vascular impedance, which is the viscous and inertial hydraulic opposition to mean and pulsatile blood flow. While distal PA remodeling, including muscularization and narrowing, increases PVR, both proximal and distal PA remodeling contribute to increases in pulmonary vascular impedance.[9,10] Analogously, while increases in PVR increase mean PA pressure, increases in impedance increase the pulmonary arterial pulse pressure as well as mean PA pressure.[6,9,11] Important consequences of proximal arterial remodeling are loss of pulmonary vascular compliance and proximal PA stiffening.

Proximal PA stiffness can predict mortality in patients with pulmonary arterial hypertension (PAH),[12-16] which is a subtype of PH. This finding has motivated clinical and basic science studies of the material properties and mechanical behavior of proximal PAs in PH.[17-32]

Here we briefly review the material properties and mechanical behaviors that have been used to assess PA stiffness, with a

Address correspondence to:
Dr. Naomi C. Chesler
Associate Professor of Biomedical Engineering
University of Wisconsin-Madison
2146 ECB, 1550 Engineering Drive
Madison, WI 53706-1609, USA
Email: chesler@engr.wisc.edu

Access this article online

Quick Response Code:	Website: www.pulmonarycirculation.org
	DOI: 10.4103/2045-8932.105040
	How to cite this article: Tian L, Chesler NC. In vivo and in vitro measurements of pulmonary arterial stiffness: A brief review. Pulm Circ 2012;2:505-17.

particular focus on proximal PAs, and then provide an in-depth discussion of the in vivo and in vitro techniques available to measure PA stiffness. In particular, we review (1) in vivo measurement of proximal PA stiffness via pressure-diameter or -cross-sectional area relationships in human, large animal and small animal models, and (2) in vitro measurement of proximal PA stiffness as well as material properties such as elastic modulus via several different testing methods that mimic one, two or several aspects of physiological loading.

DEFINITIONS

Stiffness describes the amount of force required to achieve a given deformation (or the amount of deformation that occurs in response to a given force), which is a mechanical behavior. In general, the mechanical behavior of a structure depends on the material properties, the geometry and the size or the extent of the material; thus mechanical behavior is extrinsic or extensive. Material properties, in contrast, do not depend on the size of the structure or geometry; thus material properties are intrinsic or intensive. As we describe in more detail below, material properties are calculated from relative deformation (deformation relative to a baseline state, strain) and an area-normalized force (stress). An example of an important arterial material property is elastic modulus; an important component of both geometry and size is arterial wall thickness. Therefore, two arteries composed of the same material will have the same elastic modulus no matter how large they are. In contrast, if two arteries have the same elastic moduli and the same inner diameter but one has a greater wall thickness, the thicker one will be stiffer.

A summary of commonly used parameters for material properties and mechanical behavior related to stiffness is shown in Table 1. The material properties typically used to describe arteries are the elastic modulus and incremental elastic modulus. The elastic modulus is the slope of the stress-strain behavior. However, because the stress-strain relationship of an artery is usually nonlinear, an incremental elastic modulus, defined over a particular stress or strain range is often used. Also, the elastic modulus can be calculated at a particular stress or strain. PA stiffness is frequently represented by many different parameters. The pressure-strain modulus and its inverse, dynamic compliance are reasonable metrics of stiffness and require measurements of pressure and diameter at both systole and diastole. Similarly, the stiffness coefficient and index, compliance and distensibility require measurements of pressure and diameter and/or cross-sectional area at both systole and diastole. In contrast, the relative area change (RAC) is not a true measure of stiffness. RAC depends only on the PA maximum and minimum cross-sectional areas but not pressure. Thus, a very stiff artery could exhibit a small RAC in response to a large pressure change whereas a very compliant artery could exhibit the same RAC response to a very small pressure change. A more appropriate description of RAC is "area strain" since it reflects the change in area relative to baseline area.

Table 1: Metrics commonly used to quantify pulmonary arterial stiffness and compliance

Parameter	Formula	Notes
Elastic modulus	$E = \frac{\sigma}{\varepsilon}$	The slope of stress-strain (σ–ε) curve.
Incremental elastic modulus[33]	$E_{inc} = \frac{\Delta P}{\Delta OD}\frac{2ID^2OD}{OD^2 - ID^2} + \frac{2POD^2}{OD^2 - ID^2}$	P is the pressure. ID and OD are inner and outer diameters at P, respectively. ΔP and ΔOD are the changes of pressure and outer diameter over an increment (ΔP), respectively.
Pressure-strain modulus [34]	$E_p = \frac{P_s - P_d}{ID_s - ID_d} ID_d$	
Dynamic compliance[10,35,36]	$C_{dyn} = \frac{ID_s - ID_d}{ID_d \times (P_s - P_d)} \times 10^4$	The inverse of pressure-strain modulus. Diastolic pressure (P_d) is neglected if not available.[36]
Stiffness coefficient[37,38]	$\beta_1 = \frac{\ln(P / P_r)}{ID / ID_r - 1}$	P_r is the standard (reference) pressure. ID_r and ID are the inner diameters at pressure P_r and P, respectively.
Stiffness index[15,16,28]	$\beta_2 = \frac{\ln(P_s / P_d)}{(A_{max} - A_{min}) / A_{min}}$	Luminal area (A) measured directly or estimated from ID.
Compliance[39,40]	$C = \frac{A_{max} - A_{min}}{P_s - P_d}$	
Distensibility[39,41-43]	$D = \frac{A_{max} - A_{min}}{A_{min} \times (P_s - P_d)}$	
Relative area change[12,15,28]	$RAC = \frac{A_{max} - A_{min}}{A_{min}}$	

s: systolic;**d:** diastolic

Note that the units of the parameters listed in Table 1 are not identical. Which parameters are more diagnostically and/or prognostically useful in the pulmonary circulation remains unclear.

IN VIVO MEASUREMENT

To assess proximal PA stiffness in vivo, the pressure and inner or outer diameter or cross-sectional area of proximal PAs must be measured. Ideally, these measurements are made simultaneously but they can also be done sequentially and then synchronized with the heart rate (via ECG or EKG). Since the physiological pressure range in the pulmonary circulation is generally small, resulting in a limited pressure-diameter/cross-sectional area curve, vasodilator and/or vasoconstrictor drugs are often used to shift the pressure such that the pressure-diameter/cross-sectional area relationship can be examined in a different range. In this section, we will review several techniques used to obtain in vivo measurements of pressure and inner or outer diameter data or cross-sectional area of proximal PAs in human, and large and small animals.

In vivo measurements in humans

In vivo pulmonary artery pressure measurement. The gold standard for measuring pulmonary artery pressure (PAP) is right heart catheterization (RHC). With a catheter positioned in proximal PA, the pulmonary pressure waveform can be obtained. Invasive RHC can provide accurate measurements of systolic, diastolic and mean PAP with high fidelity solid state catheters. Fluid-filled catheters are more typically used clinically but these can introduce errors in the pressure waveform due to zero leveling, damping and insufficient frequency response of the catheter.[44-46]

Noninvasively, the peak systolic PAP can be estimated by measurement of the tricuspid regurgitant (TR) jet velocity via continuous wave Doppler.[36,47] This noninvasive technique is sufficient when only peak systolic PA pressure is used to estimate stiffness, e.g., dynamic compliance defined by Dyer et al.[36] Nevertheless, this approach has its limitations. Not all individuals have easily identifiable and measureable TR Doppler jet envelope, which precludes systolic PAP measurement in some subjects.[36,47] Moreover, this method cannot be used to measure the pressure-strain modulus, PA compliance, or other metrics that require the diastolic PAP, unless the diastolic pressure is estimated from diastolic pulmonary regurgitation velocity or the relationship between systolic and diastolic pressures. However, these estimates are typically less accurate than comparable systolic pressure estimates.[13,47]

In vivo pulmonary artery diameter or cross-sectional area measurement. Decades ago, open-chest surgery was performed to measure PA diameter changes over the cardiac cycle. With the PA exposed, an electrical strain-gauge caliper was sutured to the PA adventitia as close to the true diameter as possible and the relative movement of two legs of the caliper induced a change in electrical resistance which was then converted to PA diameter.[48,49] This approach obviously is not practical for routine clinical use.

As imaging techniques have advanced in the ensuing years, several noninvasive methods have been developed that are suitable for measuring PA diameter. For example, cine-angiography has been used to obtain closed-chest diameter measurements of the right PA.[50,51] This technique requires contrast injection but allows sufficient time resolution to obtain both diastolic and systolic diameter measurements of the right PA.[51] According to Jarmakani et al., measurement of the right PA diameter is preferred over the left or main because of its relatively cylindrical shape and easily identifiable fixed points during both systole and diastole.[52]

Computed tomography (CT) has been used to obtain time-averaged main PA diameter with or without intravenous contrast medium,[53-56] but this technique is not fast enough, to date, to obtain non-time-averaged systolic and diastolic diameter measurements.[57]

PA diameter can be also obtained from standard transthoracic echocardiogram[36,58] with good temporal accuracy and reasonable spatial accuracy depending on the sound wave frequency produced by the transducer.[59]

Intravascular ultrasound (IVUS) method has been used widely as well. With an ultrasound catheter positioned in PA, the inner edge of the artery can be visualized and the inner circumference of the artery at each location can then be measured.[12,35,60-62] Moreover, the PA wall thickness can be obtained from the ultrasound images if both modalities are used simultaneously.[63,64] IVUS provides a minimally invasive means to track arterial wall motion[65] and can reach higher spatial resolution than conventional external 2-dimensional ultrasound, i.e., transthoracic echocardiography.[35] Nevertheless, IVUS has been shown to slightly overestimate the true diameter.[35,66,67]

The color Motion-Mode (CMM) Doppler tissue imaging (DTI) method was developed several years ago to measure instantaneous diameter. In this method, the DTI mode is activated in B-mode imaging to examine PA motion and then changed to CMM mode with the beam line perpendicular to the PA's superior and inferior walls. This is a two-dimensional Doppler echocardiographic measurement of instantaneous diameter combining both CMM and DTI and can provide higher spatial (1.6-1.9 mm) and temporal (5 milliseconds) resolution than conventional echocardiography.[36]

Finally, phase-contrast magnetic resonance imaging (MRI) can be used to measure cross-sectional area of the main, right and left extralobar PAs with a temporal resolution as high as 35 ms with modern techniques,[15,16,27,28,31,32,68] which is sufficient to obtain systolic and diastolic measurements. The inner diameter is then estimated from the cross-sectional area by assuming a circular cross-section. While MRI can provide accurate measurements of PA diameter, it is expensive. Also, while the temporal resolution is higher than CT, it is lower than echocardiography and IVUS.

In vivo measurements in large animals

In vivo pulmonary artery pressure measurement. To obtain in vivo PAP measurements in large animals, RHC can be performed with techniques similar to those used humans.[22,32,69,70-73]

Other invasive methods have also been developed. A one-step method is to insert a pressure microtransducer, fluid-filled catheter or high fidelity solid state pressure transducer directly into PA in an open-chest procedure.[43,74,75] To make sure there is no leaking from the stab wound in PA, the incision is typically kept quite small. This method is easy to perform but is only suitable for non-survival experiments.

As in humans, noninvasive measurement of the TR jet velocity can be used to estimate systolic PAP; however, this approach has the same limitations noted above for humans. Recently, our group described a novel correlation between stroke volume and relative area change (RAC) that allowed us to calculate PA pulse pressure in dogs with acute PH using only noninvasive imaging techniques.[32] However, this approach has not been validated in a chronic model of PH or humans.

In vivo pulmonary artery diameter or cross-sectional area measurement. In animal models, invasive methods to measure PA diameter have been employed frequently. Similar to the invasive method that was used in human decades ago,[49] an electrical recording caliper has been sutured to opposite sides of the main PA wall in dog with the chest open and main PA exposed.[76,77] The electrical recording caliper was later replaced with two miniature ultrasonic, piezoelectric crystal transducers that were sutured to the adventitia of the main PA.[43,74,75,78,79] The transit time of the ultrasonic signal is converted into distance (outer diameter of PA) through the sonomicrometer. Note that these measurements with electrical calipers or piezoelectric crystals only provide the outer diameter of the PA.

Another invasive approach is the conductance method in which the cross-sectional area of the PA is obtained by measuring the conductance of the tissue (PA) surrounding the catheter and then converting the conductance to area.[80] This method was found to correlate well with IVUS on piglet aortas.[80] IVUS has also been used to measure PA cross-sectional area and diameter in large animals.[81]

Noninvasive transthoracic echocardiogram measurement can be applied to large animals to obtain PA diameter, although this method is not frequently used. The noninvasive CMM DTI technique described above has been used in large animals such as neonatal calves to obtain inner diameter of main PA.[22,30] As mentioned above, the technique can provide high spatial and temporal resolution, which is sufficient to accurately measure main, right and left PA diameters over a cardiac cycle in large animals. Recently, our group has used MRI to measure the cross-sectional area of proximal PAs in dogs[31,32] as well as echo (unpublished data). In particular, 2D phase contrast images were acquired to obtain cross-sectional area of proximal PAs at 20 time points over the cardiac cycle with a spatial resolution ~1.6 mm, which is sufficient to obtain diastolic and systolic diameters of the main, right and left PAs.

In vivo measurement in small animals

In vivo pulmonary artery pressure measurement. The small size of rodents raises difficulties in performing RHC. However, minicatheters have been available since 1950[82] and used in the rat and mouse for RHC since 1972[83] and 2000,[84] respectively.

In rats, more RHC approaches have been successful likely due to their larger size compared to mice. Many catheters have been developed and used in rats; examples include a fluid-filled catheter with a pigtail shape contained in a well-fitting cannula,[83] a 3.5-Fr umbilical vessel catheter,[85-88] a catheter with a tip of a "shepherd's crook" shape,[89] a 3-Fr Millar catheter,[90] and a 1.4-Fr Millar catheter slipped over an introducer with a deflectable tip.[91] Depending on the catheters, different techniques have been developed to guide the catheter from right jugular or femoral vein to proximal PAs to measure PAP.

In mice, Champion et al. first used a closed chest RHC technique in mice successfully.[84,92] In this approach, a catheter with an outer diameter of 0.25 mm and a specially curved tip is passed from right jugular vein to the right heart and finally to main, right or left PA.

In studies in mice by our group, an open chest technique is used in which a 1.4 F pressure-tip catheter is introduced directly into the RV using a 20-gauge needle. After RV pressure readings are obtained, the catheter is advanced to main PA for systolic, diastolic and mean PAP measurement.[24,93] Whether or not the open-chest condition causes changes in PAP is unclear.

Finally, the magnitude of the TR jet velocity from noninvasive ultrasound has been used to estimate systolic PA pressure

in rabbits;[94] but as noted above, only an estimate of the systolic PAP can be obtained.

In vivo pulmonary artery diameter measurement. Due to the difficulties and relatively large spatial errors in measurement of proximal PA diameter in small animals, few in vivo studies have been performed. Nevertheless, recently our group has measured the inner diameter of main PA in mouse from transthoracic echocardiography with imaging system precision of 80 μm.[93] New techniques and improvement in instrumentation are still required to make these measurements feasible, easier and more accurate in small animals. For example, with smaller-sized ultrasound catheters, IVUS could be a superior technique.

IN VITRO MEASUREMENT

There exist many in vitro mechanical testing methods for quantifying the mechanical behavior and material properties of arterial tissue. Many provide only material properties whereas other provide only mechanical behaviors; few techniques allow precise measurement of both in multiple directions (i.e., axial and circumferential). In addition, to predict the material properties at a stress or strain not tested, or the mechanical behavior at a pressure or diameter (or length) not tested, a constitutive model which mathematically describes the arterial material properties and initial geometry is usually employed. In this section, we will first briefly discuss the strain-energy function that is used in a constitutive model and then detail how to obtain the initial geometry or zero-stress state. With this background in place, we will review the most common in vitro testing methods used to measure PA stiffness.

Strain-energy function

Biological materials are composite structures made up of multiple components and arranged in multiple layers. However, if we treat biological materials as a continuum, i.e., as homogenous structures with continuous properties, the concepts of stress, strain and energy in continuum mechanics can be applied and permit relatively simple mathematical analysis.[95] A strain-energy function (SEF), which describes the strain energy per unit volume stored in a material, can be written as

$$\psi = \psi(E), \qquad \text{(Eq. 1)}$$

where E is the Green-Lagrange strain that describes the deformation of the material relative to a baseline state. For example, if a bar of an initial length L_0 is stretched to a new length L, the stretch ratio is $\lambda = L/L_0$, and the Green-Lagrange strain can be calculated as $(\lambda^2 - 1)/2$. With a SEF, the strain can be related to the stress, which is the force per unit cross-sectional area required to cause that deformation.

Many different strain-energy functions have been proposed for arteries. A detailed review is beyond the scope of this paper and details can be found elsewhere.[95-99] In general, the shear strains and stresses, which describe the twisting deformation and twisting forces per unit area respectively, are not considered. Therefore, the SEF can be expressed as a function of the strain in three directions as $\psi = \psi(E_{rr}, E_{\theta\theta}, E_{zz})$, where $E_{rr}, E_{\theta\theta}, E_{zz}$ are the Green-Lagrange strains in the radial, circumferential, and longitudinal directions of an artery, respectively.

For an incompressible material, the SEF can be further simplified and expressed in a two-dimensional form as $\psi = \psi(E_{rr}, E_{\theta\theta})$ and the Cauchy stresses can be calculated as[100,101]

$$\sigma_{\theta\theta} - \sigma_{rr} = \lambda_\theta^2 \frac{\partial \psi}{\partial E_{\theta\theta}}, \ \sigma_{zz} - \sigma_{rr} = \lambda_z^2 \frac{\partial \psi}{\partial E_{zz}} \qquad \text{(Eq. 2)}$$

where λ_θ and λ_z are the stretch ratios in the circumferential and longitudinal directions, respectively, and $E_{\theta\theta} = (\lambda_\theta^2 - 1)/2$ and $E_{zz} = (\lambda_z^2 - 1)/2$.

When the artery is loaded with an internal pressure but without traction on the outer surface, the pressure can be obtained by integrating the equilibrium equation in the radial direction as[96]

$$P = \int_{r_i}^{r_o} (\sigma_{\theta\theta} - \sigma_{rr}) \frac{dr}{r}, \qquad \text{(Eq. 3)}$$

where r_i and r_o are the inner and outer radii of the artery at pressure P. Substituting Eq. 2 into Eq. 3, the pressure-diameter curve of a pressurized artery can be obtained. Finally, the pressure-diameter relationship can be used to calculate the mechanical behavior of the artery for comparison with in vivo measurements to validate the constitutive model.

Morphometry and residual strain measurement

Measurements of arterial morphometry such as wall thickness and inner and/or outer diameters are required to quantify the mechanical behavior of artery. However, quite often we can not measure the geometry at a specific pressure in vitro due to the shortness of the PA itself (e.g., main PA) or due tissue availability because the tissue may be dissected into several parts for different studies. Typically, the morphometry of a PA ring only is measured at the unloaded state, i.e., at zero internal pressure and zero longitudinal force (Fig. 1A).

It is well known that residual strain exists in an artery ring at an unloaded state. When an artery ring is cut radially, it opens as shown in Figure 1B. The opened artery is generally taken

as the stress- or strain-free state. Compared to the opened artery ring, the closed artery ring has different inner and outer circumferences and the deformation results in residual strain in the closed artery ring. This deformation is in the circumferential direction and the residual strain is called circumferential residual strain. Although small, the residual strain can have a large effect on the strain distribution across the artery wall at the physiological pressure.[30,96,102-104] It is important to note that residual strain exists in the circumferential, longitudinal and radial directions but those in the circumferential direction are typically considered the most important. To release circumferential residual strain, one well-accepted way is to cut the ring along a single radius (Fig. 1B).[105] When the artery ring is opened with a single cut, the opening angle (OA) is obtained by measuring the angle between the two lines connecting the middle point of the inner arterial wall to the edges of the open sector (Fig. 1B). The OA can be linked to the histological and mechanical properties of artery.[29]

Since arteries have three layers, each with different constituents evident by histology, the circumferential residual strain may not be fully released by one radial cut. Indeed, the residual strains in each layer may be different. To measure these, the three layers need to be separated. This process can also release longitudinal residual strain, which can be measured by comparing the length of each separated layer to the length of the intact longitudinal arterial strip.[106] However, the process of separating the media from the adventitia is technically difficult and can cause damage. Thus, the circumferential and longitudinal residual strains in different artery layers are generally not considered. The morphometry of an artery cut once radially is usually taken as the reference state for stretch or strain calculations.

Uniaxial tensile test

A uniaxial test is a procedure in which a rectangular strip cut out of an artery is pulled in one direction, usually along the longest length direction of the artery sample (Fig. 2A). In general, the artery sample is prepared as a long rectangle and uniaxial loading is performed in the circumferential or longitudinal direction. In traditional mechanics, samples to be tested in this way are cut in a dog bone shape with the center narrower than the edges to reduce boundary effects, but this is typically not done for arteries because tissue size is limited. A length to width ratio of at least 5:1 is generally considered sufficient to ignore boundary effects. The tissue sample is then mounted in the testing system with both ends of the sample held by grips or hooks and immersed in a physiological solution (PBS, PSS or PSS with drug) at the physiological temperature. The force on the artery sample is measured by a load cell and recorded simultaneously with the displacement of the grip or hook. While hard materials such as bone and metal can be tested in this configuration in both compression and tension, arteries can only be tested

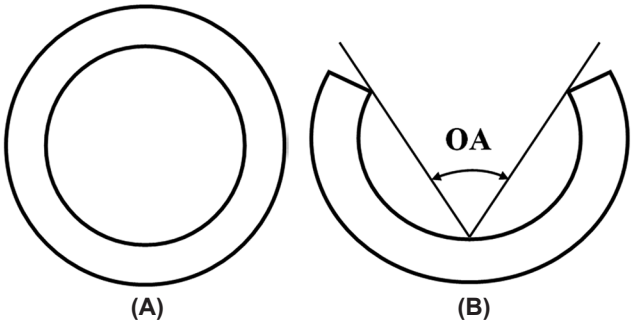

Figure 1: Schematics of **(A)** a closed artery ring and **(B)** an opened artery ring after one radial cut.

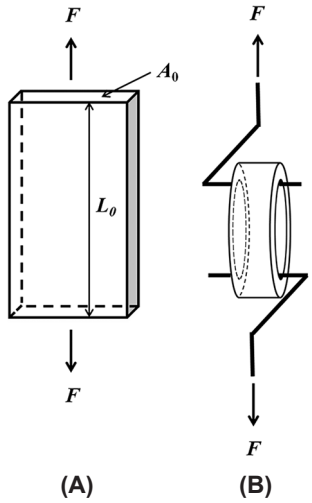

Figure 2: Schematics of **(A)** uniaxial tensile test and **(B)** ring/tension test.

in tension. As such, this test is more accurately termed as uniaxial tensile test.

In general, the sample undergoes five or more loading and unloading cycles at a constant stretch rate for preconditioning, and the force-displacement data are taken from the last loading cycle. Then, with force and displacement obtained, the Cauchy stress (σ) and Green-Lagrange strain (E) can be calculated as

$$\sigma = \frac{F\lambda}{A_0}, E = \frac{1}{2}(\lambda^2 - 1), \quad \text{(Eq. 4)}$$

where F is the force, A_0 is the cross-sectional area of the sample at the unloaded condition, and λ is the stretch ratio in the loading direction, which is calculated as ratio of the deformed (loaded) to undeformed (unloaded) lengths (L and L_0, respectively) of the sample, i.e., $\lambda = L/L_0$. The elastic modulus as a function of strain can be obtained directly from the stress-strain curve as the slope at a given strain.

To predict behavior under conditions not directly measured in a uniaxial tensile test (e.g. under biaxial

stretch), a strain energy function can be used. Assuming the artery is homogeneous and incompressible with a strain-energy function in a two-dimensional form as $\psi = \psi(E_{\theta\theta}, E_{ZZ})$ with $E_{\theta\theta}$ and E_{ZZ} denoting for the Green-Lagrange strains in the circumferential and longitudinal directions, respectively, and with shear strains neglected, the stresses can be expressed as in Eq. 2. In this case, the stress in the radial direction σ_{rr} is zero in the uniaxial tensile test. When the sample is loaded in circumferential direction, the force and stress in the longitudinal direction are also zero ($F_z = 0$; $\sigma_{ZZ} = 0$). When the sample is loaded in the longitudinal direction, the longitudinal stress is non-zero but the circumferential stress is zero ($\sigma_{\theta\theta} = 0$). By fitting the idealized stress-strain relationship expressed as in Eq. 2 to the measured stress-strain data for both circumferential and longitudinal strip samples, all material parameters in the SEF can be obtained. Finally, the stress-strain relationship at different stretch conditions can be calculated and the pressure-diameter relationship can be predicted for additional proximal PA stiffness calculations.

With the appropriate apparatus at hand, the uniaxial tensile test is easy to perform, and the sample preparation only requires a small strip, which is frequently feasible. The testing system can also be used to perform creep or stress-relaxation tests in which the strain as a function of time is measured under a constant stress or the stress as a function of time is measured under a constant strain, respectively. These two tests can provide the viscoelastic properties of an artery, which affects hemodynamic pulse wave damping. Nevertheless, some disadvantages exist. First, cutting an artery into a rectangular strip may disturb the structural integrity at the lateral edges of the strip, which could affect the validity of the measured stress and strain.[107] In addition, in the above calculation of stress (Eq. 4), the artery is assumed homogeneous and thus ignores potential differences in structure and function between the intima, media and adventitia. Finally, the uniaixal tensile test cannot fully characterize the anisotropic (directionally-dependent) material properties of an artery.[100,108] That is, the uniaxial tensile test can only provide stress-strain data in one direction per sample, with the other two directions free of force, which is not physiological. In vivo, an artery is loaded three-dimensionally.

Ring/tension test

In the ring/tension test, an artery ring is pulled by two appropriate hooks or clips which go through the lumen of the artery ring as shown in Figure 2B.[109] With the force and displacement recorded, the circumferential stress is calculated as

$$\sigma_{\theta\theta} = \frac{F\lambda}{2A_0}, \qquad \text{(Eq. 5)}$$

where F is the force, A_0 is the cross-sectional area of the sample at the unloaded condition, and λ is the stretch ratio in the circumferential direction. The factor 2 accounts for the two sides of the ring that are loaded simultaneously. The circumferential strain is calculated as in Eq. 4. Again, the artery is assumed to be homogeneous. This type of testing system can be used to test large or small PAs,[109] which is an important advantage over the uniaxial test in which typically only larger arteries can be gripped in the testing system. To obtain stress-strain information at different loading conditions, a SEF needs to be used as in the uniaxial tensile test. However, since longitudinal testing is not possible, one must assume that the stress-strain relationship is the same for both circumferential and longitudinal directions.

This test is relatively easy to perform and has the same advantages as the uniaxial tensile test and the same limitations. Most often this type of test is used to measure the forces induced by contraction and relaxation due to smooth muscle cells activation and endothelial cell signaling.[109-111]

Biaxial test

For a biaxial mechanical test, a rectangular or nearly square thin, flat (i.e., planar) sample of artery is pulled in two directions simultaneously (Fig. 3). For arterial tissue, these two directions are usually the circumferential and longitudinal directions. The artery sample is prepared with the directions of the edges corresponding to the longitudinal and circumferential directions. The stretch or strain in both circumferential and longitudinal directions are typically obtained optically by measuring the relative displacement of four small pre-marked dots in the middle region of the planar tissue sample surface, generally the intimal surface.[108] With the forces in both directions measured, the stresses can be calculated as

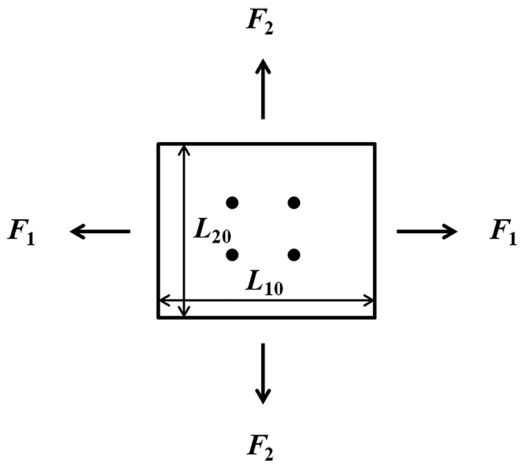

Figure 3: Schematic of biaxial test.

$$\sigma_{11} = \frac{F_1 \lambda_1}{L_{20} T_0}, \sigma_{22} = \frac{F_2 \lambda_2}{L_{10} T_0}, \quad \text{(Eq. 6)}$$

where F_1 and F_2 are the forces in direction 1 and 2 respectively, L_{10} and L_{20} are the lengths of the unloaded sample in direction 1 and 2 respectively, and T_0 is the thickness of the unloaded sample. Similar to the uniaxial test, additional PA stiffness parameters can be calculated using an SEF based on fitting the measured stress-strain data.

Compared to the uniaxial tensile test, the biaxial test is better able to characterize the anisotropic behavior of an artery, since both circumferential and longitudinal directions are loaded simultaneously.[100,108] Also, the applied force and thus amount of stretch in each direction (circumferential and longitudinal) can be controlled, allowing the simulation of in vivo stretch states under physiological conditions. Limitations include some experimental and theoretical issues. Experimentally, the problems include difficulty in gripping the tissue without inducing damaging and applying constant forces along sample edge.[108] Theoretically, the stress calculation requires the assumption of homogeneity whereas in fact the artery is generally heterogeneous. Additionally, the homogeneity of deformation within the specimen is questionable and thus the region in which the marked dots are placed for stretch measurement should be small and far away from the outer edge to reduce boundary effects.[108,112] Finally, the artery at its zero-stress state could be curved and thus the prepared tissue sample is generally not perfectly planar. As a result, the true stretch may be not uniform through arterial wall thickness due to the bending of the non-planar tissue sample during the biaxial test. Such non-uniform deformation is not accounted for in the stretch or subsequent material property calculations.

Bubble test

In the bubble test, a planar artery section is mounted on a circular channel filled with physiological solution that allows pressure inflation from one side (Figures 4A and B). The deformed artery dimensions under different inflation pressures (Fig. 4C) are then measured from images captured by at least two cameras at different angles.[17,18,113] For this test, it is important to obtain an artery sample with uniform thickness and a section large enough that the diameter of the sample region under pressure is at least 10 times the thickness of the sample.[17,113,114] During inflation, the shape of the artery section becomes ellipsoid and the stretch can be estimated by measuring the arc length before and after inflation in both circumferential and longitudinal directions. Combined with the inflation pressure, the ellipsoidal geometry data (vertical semi-axis, horizontal semi-axis, etc) are used to calculate the stresses in the two directions. Details can be found elsewhere.[17,18,115] This test is similar to the biaxial test since both circumferential and longitudinal directions are stretched simultaneously. To obtain the stress-strain data at different pressure/stretch conditions and pressure-diameter data, a SEF can be used, as in the biaxial test.

One advantage of this test is that it can be used to calculate stress-strain data in both circumferential and longitudinal directions simultaneously. This test is also suitable for curved planar samples, which is not true for the in-plane biaxial test described above or the whole artery inflation/deflation test described below. Another advantage of this test is that it is suitable for particularly short arteries, such as the main PA, which could not be tested in a whole artery inflation/deflation test without significant end effects. However, this test also has its limitations.

First, as mentioned above, the test requires a thin, flat sample, which may not be possible to obtain in diseased states. Second, the sample is loaded equally in the circumferential and longitudinal directions and the loading cannot be independently controlled.[116] Third, the data collection and analysis techniques are typically more complicated than some other methods.[117] Moreover, this test is only suitable for quasi-static testing since the image

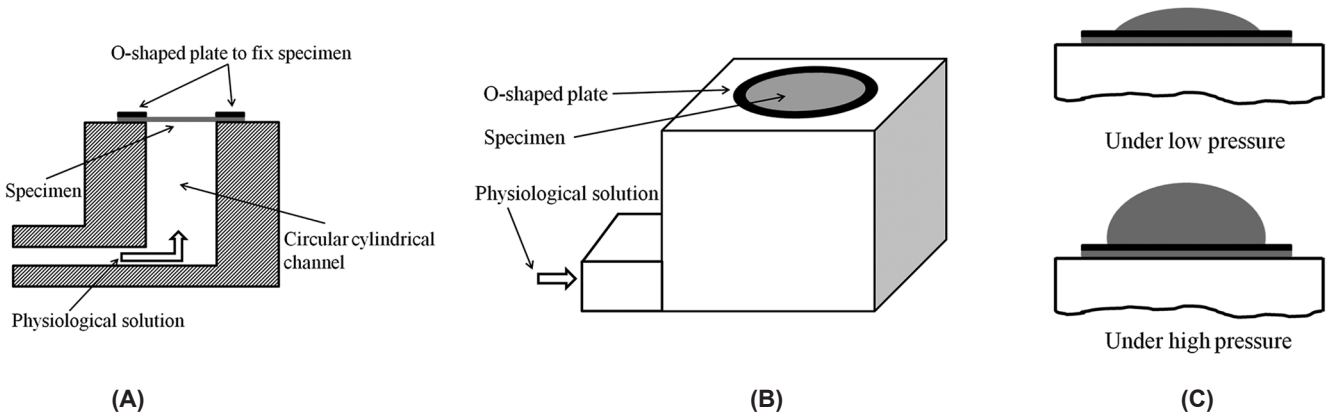

Figure 4: Schematics of **(A)** sectional view of bubble test fixture; **(B)** perspective view of the fixture; and **(C)** the inflation of artery membrane under pressure.

of the inflated artery cannot be captured with high quality at high frequencies with currently available equipment. Nevertheless, this can be improved in principle with improved imaging systems. Finally, the shear behavior can be not captured[117] and tissue samples must be sufficiently intact, and have no holes or leaks, that they can withstand pressurization.

Inflation-force test

A third type of biaxial test is the inflation-force (or tension) test. In this case, a whole artery with no side branches is pressurized at a fixed axial length or stretched at a fixed pressure (Fig. 5). One widely used testing system is the pressure myograph (Danish Myotechnology). This system has a pressure transducer at each end of the artery specimen and a force transducer on one end (on the cannula used to mount the tissue to the system). A CCD camera above or below the specimen is used to measure arterial diameter and often wall thickness, depending on the optical density of the tissue. Thus, pressure, axial force, diameter and often wall thickness can be measured simultaneously. One limitation of this system is the time resolution of the data acquisition.

To address these limitations and allow collection of frequency-dependent material properties, our group has developed a system that combines a high-frequency dynamic pump with a CCD camera and high-frequency amplifiers for the pressure transducers.[118] The CCD camera is able to capture images at a frequency of at least 20 Hz, from which the outer diameter can be measured with commercial software (IonOptix). The amplifiers are able to measure pressure without frequency-dependence in amplitude up to 100 Hz and only a slight phase delay above 20 Hz. Currently, however, this system uses an arteriograph that does not integrate a force transducer (Living Systems Instrumentation) and thus does not provide axial force data.

Depending the testing system, then, the internal pressure, outer diameter (or inner diameter), and/or the axial force are measured simultaneously during an inflation/force test. The internal pressure (P) and the measured axial force (F) can be expressed as functions of the circumferential, radial and longitudinal stresses ($\sigma_{\theta\theta}$, σ_{rr} and σ_{zz}, respectively)[96]

$$P = \int_{r_1}^{r_0} (\sigma_{\theta\theta} - \sigma_{rr}) \frac{dr}{r}, \qquad F = \pi \int_{r_i}^{r_0} [2(\sigma_{zz} - \sigma_{rr}) - (\sigma_{\theta\theta} - \sigma_{rr})] r dr. \qquad \text{(Eq. 7)}$$

At a fixed pressure, the axial force varies with the longitudinal stretch. Although the axial force-stretch relationship can indicate the material behavior in the axial (or longitudinal) direction, it does not provide proximal PA stiffness as typically defined. Thus this behavior is not discussed here. At a fixed axial stretch, the pressure and diameter relationship can directly provide relative area change (RAC), compliance and distensibility defined as in Table 1. To estimate the stress-strain relationship, the SEF can be employed. In particular, with geometry data and the zero-stress state geometry (reference state) as well as the assumption of incompressibility, the circumferential stretch can be estimated for a given longitudinal stretch under different pressures. The radial stretch can be calculated with the incompressibility condition. Fitting the SEF to the tested data by substituting Eq. 2 into Eq. 7 enables calculation of the material properties, which then can be used to generate the stress-strain or pressure-diameter relationship.

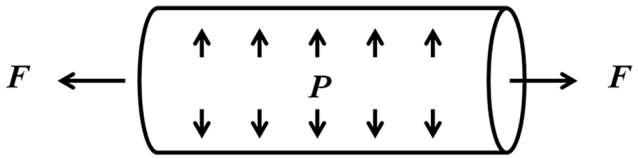

Figure 5: Schematic of inflation-force test.

Alternatively if the artery is assumed to be homogeneous and isotropic (with directionally-independent material properties), the circumferential stress at a point (r) inside the artery wall can be estimated as[119]

$$\sigma_{\theta\theta}(r) = \frac{Pr_i^2}{(r_0^2 - r_i^2)}\left(\frac{r_0^2}{r^2} + 1\right), \qquad \text{(Eq. 8)}$$

where r_i and r_0 are respectively the internal and external radii of the artery at internal pressure P. For a thin-wall artery, the average circumferential stress can be simply estimated as[95]

$$\sigma_{\theta\theta} = \frac{Pr_i}{T}, \qquad \text{(Eq. 9)}$$

where T is the wall thickness of the artery at pressure P. Note that this stress is an average across the wall.

The dynamic inflation-force test is the best in vitro mechanical test in terms of mimicking the physiological loading condition. The measured pressure-diameter data can be directly compared to the in vivo measured data if the in vivo longitudinal stretch is used in vitro. However, the shear force exerted on the artery wall due to the blood flow in vivo is generally not considered in the in vitro test. Other issues should also be kept in mind. In particular, the artery should be long enough to reduce boundary effects (length to diameter ratio greater than five, for example). If the end-to-end length of the sutured artery tube is too long, buckling can occur, depending on the longitudinal stretch. After buckling, the longitudinal stretch increases and the measured pressure-diameter data cannot be combined with the data before buckling as a continuous curve for analysis.

Experimental challenges include the preparation of bubble-free physiological solution during perfusion, which can affect the measured data especially for high frequency tests. Like the bubble test, tissue samples must be sufficiently intact so that they can withstand pressurization.

Torsion test

In a torsion test, either a whole artery section or a planar section of an artery is twisted. For the former, in addition to an applied internal pressure and longitudinal stretch, the artery is subjected to a torque that twists the artery around the longitudinal axis (Fig. 6A).[120,121] For the latter, two types of tests have been used. One is the rotational shear test. In this test, a flat section of artery is prepared with its edge fixed on a rigid plate and center attached to another rigid disc that transfers the torque to the artery section (Fig. 6B).[122] The other one is the simple shear test. In this test, a cuboid artery section is prepared and sandwiched between top and bottom plates. While one plate delivers the displacement, the other one measures the force (Fig. 6C).[123,124] With the torque or shear stress and the shear strain known, the shear modulus or the shear stress-strain relationship can be obtained. Detailed testing system setup and calculations can be found elsewhere.[95,120-125]

Since arteries are soft materials in general and can have large deformations, and care should be taken to ensure the artery is well attached to the plate, the rotational and simple shear tests on a planar artery are not easy to perform. The inflation/force/torsion test requires a complex testing system and this system is not often used to examine the shear stress-strain behavior of PAs. Nevertheless, the torsion or shear test was proposed as a necessary test combined with biaxial or inflation-force test to better characterize the anisotropic properties of artery.[126]

Mechanical testing after biochemical or mechanical processing

Performing mechanical tests after biochemical or mechanical processes can provide additional insight into the components of the arterial wall responsible for material properties and mechanical behaviors. For example, arteries can be processed biochemically to remove cells (i.e., decellularized) or certain proteins (e.g., collagen) prior to mechanical testing.[21,127,128] Mechanically, the artery can separated into layers based on the histology (intima, media and adventitia layers if possible) and individual layers can then be tested. Due to the difficulty of layer separation and in testing the sponge-like adventitial layer, the adventitial layer is usually trimmed and only the intima-media layer is tested. In this type of test, some characteristics of individual layers can be measured. The uniaxial tensile test has been performed on the separated intima-media layer of the main PA from adult bovines.[29] Typically, neither bubble nor inflation-force testing can be performed on either biochemically or mechanically processed tissues because they leak when perfused.

While tests after biochemical or mechanical processes can provide data and new insights, the interactions between components or layers are also eliminated and these interactions may play an important role in the overall material properties and mechanical behavior of intact arteries.[129]

SUMMARY

Proximal pulmonary arterial stiffness is an important factor contributing to RV afterload and thus could be a useful prognostic parameter for PH. Although different definitions have been proposed to obtain PA stiffness, all these calculations require pressure and/or cross-sectional area or diameter measurements. Therefore, accurate measurement or estimation of these data is important. For in vivo measurements, we have provided a review of available methods in human and large and small animal models. To measure pulmonary artery pressure, right heart catheterization is standard and often performed in human and large animals, although noninvasive echocardiography and MRI techniques are increasingly being used. For small animals, it is more common to insert a catheter directly into PA or RV in a nonsurvival surgery. To obtain the dynamic geometry of proximal PAs (cross-sectional area or diameter) over a cardiac cycle, echocardiography and MRI are currently the preferred techniques because they

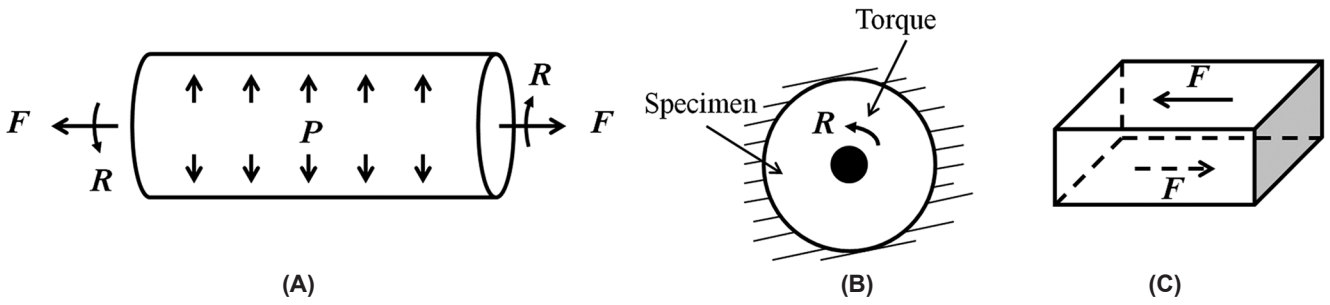

Figure 6: Schematics of **(A)** inflation/force/torsion test; **(B)** rotational shear test; and **(C)** simple shear test.

are noninvasive and have acceptable temporal and spatial resolutions, especially for humans and large animals. With improvement in spatial and temporal resolutions in the future, these techniques can be also applied to small animals. Because the physiological pressure range generally is small in the pulmonary circulation, vasoactive drugs are often given so that the pressure-diameter/cross-sectional relationship can be examined to obtain the PA's stiffness in different pressure ranges. Exercise or other interventions can achieve the same effect and could be used to more comprehensively characterize the proximal PA mechanical behavior and material properties.

In vitro, several testing methods exist to characterize the proximal PA mechanical behavior and material properties. While the uniaxial tensile and ring/tension tests are simple and easy to perform, the resulting data cannot fully characterize the anisotropic properties of PAs, and biaxial and bubble tests are better in this sense. Tests on individual layers or one or two components of artery, which are compatible with some but not all in vitro testing methods, can provide additional information. To obtain the pressure-diameter relationship and thus PA stiffness using the data from in vitro tests, an appropriate strain-energy function is usually needed. To best mimic the mechanical behavior of the proximal PA in vivo, the inflation-force test is recommended.

As reviewed here, many in vivo and in vitro measurement methods are available to measure or estimate proximal PA stiffness, each with advantages and disadvantages. Since proximal PA stiffness is an important contributor to RV afterload and eventual RV failure, its accurate measurement and proper interpretation are of clinical as well as scientific importance.

REFERENCES

1. Simonneau G, Robbins IM, Beghetti M, Channick RN, Delcroix M, Denton CP, et al. Updated clinical classification of pulmonary hypertension. J Am Coll Cardiol 2009;54:S43-54.
2. Spann JF. Contractile and pump function of the pressure-overloaded heart. In: Myocardial hypertrophy and failure, edited by Alpert NR. New York: Raven Press; 1983.
3. Durmowicz AG, Stenmark KR. Mechanisms of structural remodeling in chronic pulmonary hypertension. Pediatr Rev 1999;20:91-102.
4. Stenmark KR, Fagan KA, Frid MG. Hypoxia-induced pulmonary vascular remodeling - Cellular and molecular mechanisms. Circ Res 2006;99:675-91.
5. Voelkel NF, Quaife RA, Leinwand LA, Barst RJ, McGoon MD, Meldrum DR, et al. Right ventricular function and failure - Report of a National Heart, lung, and Blood Institute working group on cellular and molecular mechanisms of right heart failure. Circulation 2006;114:1883-91.
6. Hunter KS, Lee PF, Lanning CJ, Ivy DD, Kirby KS, Claussen LR, et al. Pulmonary vascular input impedance is a combined measure of pulmonary vascular resistance and stiffness and predicts clinical outcomes better than pulmonary vascular resistance alone in pediatric patients with pulmonary hypertension. Am Heart J 2008;155:166-74.
7. Bogaard HJ, Abe K, Noordegraaf AV, Voelkel NF. The right ventricle under pressure cellular and molecular mechanisms of right-heart failure in pulmonary hypertension. Chest 2009;135:794-804.
8. Greyson CR. The right ventricle and pulmonary circulation: Basic concepts. Rev Esp Cardiol 2010;63:81-95.
9. Grant BJ, Lieber BB. Clinical significance of pulmonary arterial input impedance. Eur Respir J 1996;9:2196-9.
10. Weinberg CE, Hertzberg JR, Ivy DD, Kirby KS, Chan KC, Valdes-Cruz L, et al. Extraction of pulmonary vascular compliance, pulmonary vascular resistance, and right ventricular work from single-pressure and Doppler flow measurements in children with pulmonary hypertension: A new method for evaluating reactivity - in vitro and clinical studies. Circulation 2004;110:2609-17.
11. Grant BJ, Paradowski LJ, Fitzpatrick JM. Effect of perivascular electromagnetic flow probes on pulmonary hemodynamics. J Appl Physiol 1988;65:1885-90.
12. Rodés-Cabau J, Domingo E, Román A, Majó J, Lara B, Padilla F, et al. Intravascular ultrasound of the elastic pulmonary arteries: A new approach for the evaluation of primary pulmonary hypertension. Heart 2003;89:311-5.
13. Mahapatra S, Nishimura RA, Oh JK, McGoon MD. The prognostic value of pulmonary vascular capacitance determined by Doppler echocardiography in patients with pulmonary arterial hypertension. J Am Soc Echocardiogr 2006;19:1045-50.
14. Mahapatra S, Nishimura RA, Sorajja P, Cha S, McGoon MD. Relationship of pulmonary arterial capacitance and mortality in idiopathic pulmonary arterial hypertension. J Am Coll Cardiol 2006;47:799-803.
15. Gan CTJ, Lankhaar JW, Westerhof N, Marcus JT, Becker A, Twisk JW, et al. Noninvasively assessed pulmonary artery stiffness predicts mortality in pulmonary arterial hypertension. Chest 2007;132:1906-12.
16. Stevens GR, Garcia-Alvarez A, Sahni S, Garcia MJ, Fuster V, Sanz J. RV dysfunction in pulmonary hypertension is independently related to pulmonary artery stiffness. JACC Cardiovasc Imaging 2012;5:378-87.
17. Drexler EA, Quinn TP, Slifka AJ, McCowan CN, Bischoff JE, Wrigth JE, et al. Comparison of mechanical behavior among the extrapulmonary arteries from rats. J Biomech 2007;40:812-9.
18. Drexler ES, Bischoff JE, Slifka AJ, McCowan CN, Quinn TP, Shandas R, et al. Stiffening of the extrapulmonary arteries from rats in chronic hypoxic pulmonary hypertension. J Res Natl Inst Stand Technol 2008;113:239-49.
19. Zhang YH, Dunn ML, Drexler ES, McCowan CN, Slifka AJ, Ivy DD, et al. A microstructural hyperelastic model of pulmonary arteries under normo- and hypertensive conditions. Ann Biomed Eng 2005;33:1042-52.
20. Zhang Y, Dunn ML, Hunter KS, Lanning C, Ivy DD, Claussen L, et al. Application of a microstructural constitutive model of the pulmonary artery to patient-specific studies: Validation and effect of orthotropy. J Biomech Eng 2007;129:193-201.
21. Lammers SR, Kao PH, Qi HJ, Hunter K, Lanning C, Albietz J, et al. Changes in the structure-function relationship of elastin and its impact on the proximal pulmonary arterial mechanics of hypertensive calves. Am J Physiol Heart Circ Physiol 2008;295:H1451-9.
22. Hunter KS, Albietz JA, Lee PF, Lanning CJ, Lammers SR, Hofmeister SH, et al. *In vivo* measurement of proximal pulmonary artery elastic modulus in the neonatal calf model of pulmonary hypertension: Development and *ex vivo* validation. J Appl Physiol 2010;108:968-75.
23. Kobs RW, Muvarak NE, Eickhoff JC, Chesler NC. Linked mechanical and biological aspects of remodeling in mouse pulmonary arteries with hypoxia-induced hypertension. Am J Physiol Heart Circ Physiol 2005;288:H1209-17.
24. Ooi CY, Wang Z, Tabima DM, Eickhoff JC, Chesler NC. The role of collagen in extralobar pulmonary artery stiffening in response to hypoxia-induced pulmonary hypertension. Am J Physiol Heart Circ Physiol 2010;299:H1823-31.
25. Tabima DM, Chesler NC. The effects of vasoactivity and hypoxic pulmonary hypertension on extralobar pulmonary artery biomechanics. J Biomech 2010;43:1864-9.
26. Wang Z, Chesler NC. Role of collagen content and cross-linking in large pulmonary arterial stiffening after chronic hypoxia. Biomech Model Mechanobiol 2012;11:279-89.
27. Sanz J, Kuschnir P, Rius T, Salguero R, Sulica R, Einstein AJ, et al. Pulmonary arterial hypertension: Noninvasive detection with phase-contrast MR imaging. Radiology 2007;243:70-9.
28. Sanz J, Kariisa M, Dellegrottaglie S, Prat-González S, Garcia MJ, Fuster V, et al. Evaluation of pulmonary artery stiffness in pulmonary hypertension with cardiac magnetic resonance. JACC Cardiovasc Imaging 2009;2:286-95.
29. Tian L, Lammers SR, Kao PH, Reusser M, Stenmark KR, Hunter KS, et al. Linked opening angle and histological and mechanical aspects of the proximal pulmonary arteries of healthy and pulmonary hypertensive rats and calves. Am J Physiol Heart Circ Physiol 2011; 301:H1810-8.
30. Tian L, Lammers SR, Kao PH, Albietz JA, Stenmark KR, Hunter KS, et al. Impact of residual stretch and remodeling on collagen engagement

in healthy and pulmonary hypertensive calf pulmonary arteries at physiological pressures. Ann Biomed Eng 2012;40:1419-33.
31. Roldán-Alzate A, Reeder SB, Francois CJ, Keevil JG, Runo JR, Chesler NC. Low MPA relative cross sectional area change correlates with decreased RV function. ATS 2010 International Conference, 2010.
32. Bellofiore A, Roldán-Alzate A, Besse M, Kellihan HB, Consigny DW, Francois CJ, et al. Impact of acute pulmonary embolization on arterial stiffening and right ventricular function in dogs. Ann Biomed Eng 2012 [Epub ahead of print]
33. Hudetz AG. Incremental elastic modulus for orthotropic incompressible arteries. J Biomech 1979;12:651-5.
34. Peterson LH, Jensen RE, Parnell J. Mechanical properties of arteries in vivo. Circ Res 1960;8: 622-39.
35. Weinberg CE, Hertzberg JR, Shandas R. Use of intravascular ultrasound to measure local compliance of the pediatric pulmonary artery: *In vitro* studies. J Am Soc Echocardiogr 2002;15:1507-14.
36. Dyer K, Lanning C, Das B, Lee PF, Ivy DD, Valdes-Cruz L, et al. Noninvasive Doppler tissue measurement of pulmonary artery compliance in children with pulmonary hypertension. J Am Soc Echocardiogr 2006;19:403-12.
37. Hayashi K, Handa H, Nagasawa S, Okumura A, Moritake K. Stiffness and elastic behavior of human intracranial and extracranial arteries. J Biomech 1980;13:175-84.
38. Kawasaki T, Sasayama S, Yagi S, Asakawa T, Hirai T. Non-invasive assessment of the age related changes in stiffness of major branches of the human arteries. Cardiovasc Res 1987;21:678-87.
39. Hayoz D, Rutschmann B, Perret F, Niederberger M, Tardy Y, Mooser V, et al. Conduit artery compliance and distensibility are not necessarily reduced in hypertension. Hypertension 1992;20:1-6.
40. Yuan JG, Hales CA, Rich S, Archer SL, West JB, editors. Textbook of Pulmonary Vascular Disease. New York: Springer; 2011.
41. Hayashi K, Naiki T. Adaptation and remodeling of vascular wall; biomechanical response to hypertension. J Mech Behav Biomed Mater 2009;2:3-19.
42. Berger RM, Cromme-Dijkhuis AH, Hop WC, Kruit MN, Hess J. Pulmonary arterial wall distensibility assessed by intravascular ultrasound in children with congenital heart disease: An indicator for pulmonary vascular disease? Chest 2002;122:549-57.
43. Santana DB, Barra JG, Grignola JC, Ginés FF, Armentano RL. Pulmonary artery smooth muscle activation attenuates arterial dysfunction during acute pulmonary hypertension. J Appl Physiol 2005;98:605-13.
44. Her C, Kosse A, Lees DE. Elevated pulmonary artery systolic storage volume associated with improved ventilation-to-perfusion ratios in acute respiratory failure. Chest 1992;102:560-7.
45. Huez S, Brimioulle S, Naeije R, Vachiéry JL. Feasibility of routine pulmonary arterial impedance measurements in pulmonary hypertension. Chest 2004;125:2121-8.
46. Gupta H, Ghimire G, Naeije R. The value of tools to assess pulmonary arterial hypertension. Eur Respir Rev 2011;20:222-35.
47. Friedberg MK, Feinstein JA, Rosenthal DN. A novel echocardiographic Doppler method for estimation of pulmonary arterial pressures. J Am Soc Echocardiogr 2006;19:559-62.
48. Mallos AJ. An electrical caliper for continuous measurement of relative displacement. J Appl Physiol 1962;17:131-4.
49. Greenfield JC, Griggs DM. Relation between pressure and diameter in main pulmonary artery of man. J Appl Physiol 1963;8:557-9.
50. Gozna ER, Marble AE, Shaw A, Holland JG. Age-related changes in the mechanics of the aorta and pulmonary artery of man. J Appl Physiol 1974;36:407-11.
51. Herve P, Musset D, Simonneau G, Wagner W Jr, Duroux P. Almitrine decreases the distensibility of the large pulmonary arteries in man. Chest 1989;96:572-7.
52. Jarmakani JM, Graham TP, Benson DW, Canent RV, Greenfield JC. *In vivo* pressure-radius relationships of the pulmonary artery in children with congenital heart disease. Circulation 1971;43:585-92.
53. Kuriyama K, Gamsu G, Stern RG, Cann CE, Herfkens RJ, Brundage BH. CT-determined pulmonary artery diameters in predicting pulmonary hypertension. Invest Radiol 1984;19:16-22.
54. Moore NR, Scott JP, Flower CD, Higenbottam TW. The relationship between pulmonary artery pressure and pulmonary artery diameter in pulmonary hypertension. Clin Radiol 1988;39:486-9.
55. Edwards PD, Bull RK, Coulden R. CT measurement of main pulmonary artery diameter. Br J Radiol 1998;71:1018-20.
56. Burger IA, Husmann L, Herzog BA, Buechel RR, Pazhenkottil AP, Ghadri JR, et al. Main pulmonary artery diameter from attenuation correction CT scans in cardiac SPECT accurately predicts pulmonary hypertension. J Nucl Cardiol 2011;18:634-41.
57. Truong QA, Massaro JM, Rogers IS, Mahabadi AA, Kriegel MF, Fox CS, et al. Reference values for normal pulmonary artery dimensions by noncontrast cardiac computed tomography: The Framingham Heart Study. Circ Cardiovasc Imaging 2012;5:147-54.
58. Wu DK, Hsiao SH, Lin SK, Lee CY, Yang SH, Chang SM, et al. Main pulmonary arterial distensibility: Different presentation between chronic pulmonary hypertension and acute pulmonary embolism. Circ J 2008;72:1454-9.
59. Coatney RW. Ultrasound imaging: Principles and applications in rodent research. ILAR J 2001;42:233-47.
60. Borges AC, Wensel R, Opitz C, Bauer U, Baumann G, Kleber FX. Relationship between haemodynamics and morphology in pulmonary hypertension. A quantitative intravascular ultrasound study. Eur Heart J 1997;18:1988-94.
61. Bressollette E, Dupuis J, Bonan R, Doucet S, Cernacek P, Tardif JC. Intravascular ultrasound assessment of pulmonary vascular disease in patients with pulmonary hypertension. Chest 2001;120:809-15.
62. Lau EM, Iyer N, Ilsar R, Bailey BP, Adams MR, Celermajer DS. Abnormal pulmonary artery stiffness in pulmonary arterial hypertension: *In vivo* study with intravascular ultrasound. PLoS One 2012;7:e33331.
63. Scott PJ, Essop AR, Al-Ashab W, Deaner A, Parsons J, Williams G. Imaging of pulmonary vascular disease by intravascular ultrasound. Int J Cardvasc Imaging 1993;9:179-84.
64. Day RW, Tani LY. Pulmonary intravascular ultrasound in infants and children with congenital heart disease. Catheter Cardiovasc Diagn 1997;41:395-8.
65. Berger RM, Cromme-Dijkhuis AH, van Vliet AM, Hess J. Evaluation of the pulmonary vasculature and dynamics with intravascular ultrasound imaging in children and infants. Pediatr Res 1995;38:36-41.
66. Sheikh KH, Davidson CJ, Kisslo KB, Harrison JK, Himmelstein SI, Kisslo J, et al. Comparison of intravascular ultrasound, external ultrasound and digital angiography for evaluation of peripheral artery dimensions and morphology. Am J Cardiol 1991;67:817-22.
67. Hardt SE, Just A, Bekeredjian R, Kübler W, Kirchheim HR, Kuecherer HF. Aortic pressure-diameter relationship assessed by intravascular ultrasound: Experimental validation in dogs. Am J Physiol 1999;276:H1078-85.
68. Kang KW, Chang HJ, Kim YJ, Choi BW, Lee HS, Yang WI, et al. Cardiac magnetic resonance imaging-derived pulmonary artery distensibility index correlates with pulmonary artery stiffness and predicts functional capacity in patients with pulmonary arterial hypertension. Circ J 2011;75:2244-51.
69. Stenmark KR, Fasules J, Hyde DM, Voelkel NF, Henson J, Tucker A, et al. Severe pulmonary hypertension and arterial adventitial changes in newborn calves at 4300 m. J Appl Physiol 1987;62:821-30.
70. Kim H, Yung GL, Marsh JJ, Konopka RG, Pedersen CA, Chiles PG, et al. Endothelin mediates pulmonary vascular remodelling in a canine model of chronic embolic pulmonary hypertension. Eur Respir J 2000;15:640-8.
71. Okada M, Yamashita C, Okada M, Okada K. A dehydromonocrotaline-induced pulmonary hypertension model in the beagle. J Thorac Cardiovasc Surg 1995;110:546-7.
72. Chen EP, Bittner HB, Craig DM, Davis RD Jr, Van Trigt P 3rd. Pulmonary hemodynamics and blood flow characteristics in chronic pulmonary hypertension. Ann Thorac Surg 1997;63:806-13.
73. Gust R, Schuster DP. Vascular remodeling in experimentally induced subacute canine pulmonary hypertension. Exp Lung Res 2001;27:1-12.
74. Johnson TA, Henry GW, Lucas CL, Keagy BA, Lores ME, Hsiao HS, et al. Two-dimensional in vivo pressure/diameter relationships in the canine main pulmonary artery. Cardiovasc Res 1985;19:442-8.
75. Bia D, Armentano R, Craiem D, Grignola J, Ginés F, Simon A, et al. Smooth muscle role on pulmonary arterial function during acute pulmonary hypertension in sheep. Acta Physiol Scand 2004;181:359-66.
76. Patel DJ, Schilder DP, Mallos AJ. Mechanical properties and dimensions of the major pulmonary arteries. J Appl Physiol 1960;15:92-6.
77. Ingram RH, Szidon JP, Fishman AP. Response of the main pulmonary artery of dogs to neuronally released versus blood-borne norepinephrine. Circ Res 1970;26:249-62.
78. Zuckerman BD, Orton EC, Stenmark KR, Trapp JA, Murphy JR, Coffeen PR, et al. Alteration of the pulsatile load in the high-altitude calf model of pulmonary hypertension. J Appl Physiol 1991;70:859-68.
79. Grant BJ, Canty JM Jr, Srinivasan G, Brody AS. Pulmonary arterial elasticity in awake dogs. J Appl Physiol 1993;75:840-8.
80. Kornet L, Jansen JR, Nijenhuis FC, Langewouters GJ, Versprille A. The compliance of the porcine pulmonary artery depends on pressure and heart

rate. J Physiol 1998;512:917-26.
81. Pandian NG, Weintraub A, Kreis A, Schwartz SL, Konstam MA, Salem DN. Intracardiac, intravascular, two-dimensional, high-frequency ultrasound imaging of pulmonary artery and its branches in humans and animals. Circulation 1990;81:2007-12.
82. Gauer OH, Gienapp E. A miniature pressure-recording device. Science 1950;112:404-5.
83. Herget J, Palecek F. Pulmonary arterial blood pressure in closed chest rats changes after catecholamines, histamine and serotonin. Arch Int Pharmacodyn Ther 1972;198:107-17.
84. Champion HC, Villnave DJ, Tower A, Kadowitz PJ, Hyman AL. A novel right-heart catheterization technique for in vivo measurement of vascular responses in lungs of intact mice. Am J Physiol Heart Circ Physiol 2000;278:H8-15.
85. Stinger RB, Iacopino VJ, Alter I, Fitzpatrick TM, Rose JC, Kot PA. Catheterization of the pulmonary artery in the closed-chest rat. J Appl Physiol 1981;51:1047-50.
86. Oka M, Morris KG, McMurtry IF. NIP-121 is more effective than nifedipine in acutely reversing chronic pulmonary hypertension. J Appl Physiol 1993;75:1075-80.
87. Voelkel NF, Tuder RM, Bridges J, Arend WP. Interleukin-1 receptor antagonist treatment reduces pulmonary hypertension generated in rats by monocrotaline. Am J Respir Cell Mol Biol 1994;11:664-75.
88. Janssens SP, Bloch KD, Nong Z, Gerard RD, Zoldhelyi P, Collen D. Adenoviral-mediated transfer of the human endothelial nitric oxide synthase gene reduces acute hypoxic pulmonary vasoconstriction in rats. J Clin Invest 1996;98:317-24.
89. Hayes BE, Will JA. Pulmonary artery catheterization in the rat. Am J Physiol Heart Circ Physiol 1978;235:H452-4.
90. Zierhut W, Zimmer HG. Effect of calcium antagonists and other drugs on the hypoxia-induced increase in rat right ventricular pressure. J Cardiovasc Pharmacol 1989;14:311-8.
91. Deten A, Millar H, Zimmer HG. Catheterization of pulmonary artery in rats with an ultraminiature catheter pressure transducer. Am J Physiol Heart Circ Physiol 2003;285:H2212-7.
92. Champion HC, Bivalacqua TC, Greenberg SS, Giles TD, Hyman AL, Kadowitz PJ. Adenoviral gene transfer of endothelial nitric-oxide synthase (eNOS) partially restores normal pulmonary arterial pressure in eNOS-deficient mice. Proc Natl Acad Sci USA 2002;99:13248-253.
93. Tabima DM, Roldan-Alzate A, Wang Z, Hacker TA, Molthen RC, Chesler NC. Persistent vascular collagen accumulation alters hemodynamic recovery from chronic hypoxia. J Biomech 2012;45:799-804.
94. Chow MJ, Zou Y, He H, McGowan FX, Zurakowski D, Zhang Y. Obstruction-induced pulmonary vascular remodeling. J Biomech Eng 2011;133:111009.
95. Fung YC. Biomechanics: Mechanical Properties of Living Tissues. New York: Springer-Verlag; 1993.
96. Holzapfel GA, Gasser TC, Ogden RW. A new constitutive framework for arterial wall mechanics and a comparative study of material models. J Elasticity 2000;61:1-48.
97. Humphrey JD. Cardiovascular Solid Mechanics. Cells, Tissues, and Organs. New York: Springer-Verlag; 2002.
98. Holzapfel GA. Collagen in Arterial Walls: Biomechanical Aspects. In: Collagen: Structure and Mechanics, In: Fratzl P, editor. New York: Springer; 2008.
99. Kao PH, Lammers S, Tian L, Hunter K, Stenmark KR, Shandas R, et al. A microstructurally-driven model for pulmonary artery tissue. ASME J Biomech Eng 2011;133:051002.
100. Humphrey JD. Mechanics of arterial wall: Review and directions. Crit Rev Biomed Eng 1995;23:1-162.
101. Tian L. Bioengineering investigations of pulmonary vascular function in pulmonary hypertension: *In vivo*, in vitro and modeling studies. Ph.D. Thesis. University of Colorado at Boulder; 2010.
102. Chuong CJ, Fung YC. On residual stresses in arteries. ASME J Biomech Eng 1986;108:189-92.
103. Fung YC. What are the residual stresses doing in our blood vessels? Ann Biomed Eng 1991;19:237-49.
104. Rachev A, Greenwald SE. Residual strains in conduit arteries. J Biomech 2003;36:661-70.
105. Fung YC, Liu SQ. Change of residual strains in arteries due to hypertrophy caused by aortic constriction. Circ Res 1989;65:1340-9.
106. Holzapfel GA, Sommer G, Auer M, Regitnig P, Ogden RW. Layer-specific 3D residual deformations of human aortas with non-atherosclerotic intimal thickening. Ann Biomed Eng 2007;35:530-45.
107. Holzapfel GA. Determination of material models for arterial walls from uniaxial extension tests and histological structure. J Theor Biol 2006;238:290-302.
108. Sacks MS, Sun W. Multiaxial mechanical behavior of biological materials Annu Rev Biomed Eng 2003;5:251-84.
109. Ko EA, Song MY, Donthamsetty R, Makino A, Yuan JX. Tension measurement in isolated rat and mouse pulmonary artery. Drug Discov Today Dis Models 2010;7:123-30.
110. Kunichika N, Yu Y, Remillard CV, Platoshyn O, Zhang S, Yuan JX. Overexpression of TRPC1 enhances pulmonary vasoconstriction induced by capacitative Ca2+ entry. Am J Physiol Lung Cell Mol Physiol 2004;287:L962-9.
111. Xu M, Platoshyn O, Makino A, Dillmann WH, Akassoglou K, Remillard CV, et al. Characterization of agonist-induced vasoconstriction in mouse pulmonary artery. Am J Physiol Heart Circ Physiol 2008;294:H220-8.
112. Sun W, Sacks MS, Scott MJ. Effects of boundary conditions on the estimation of the planar biaxial mechanical properties of soft tissues. J Biomech Eng 2005;127:709-15.
113. Drexler ES, Slifka AJ, Wright JE, McCowan CN, Finich DS, Quinn TP, et al. An experimental method for measuring mechanical properties of rat pulmonary arteries verified with latex. J Res Natl Inst Stand Technol 2003;108:183-91.
114. Young WC, Budynas RG. Roark's Formulas for Stress and Strain. New York: McGraw-Hill; 2002.
115. Bischoff JE, Drexler ES, Slifka AJ, McCowan CN. Quantifying nonlinear anisotropic elastic material properties of biological tissue by use of membrane inflation. Comput Methods Biomech Biomed Engin 2009;12:353-69.
116. Hsu FP, Liu AM, Downs J, Rigamonti D, Humphrey JD. A triplane video-based experimental system for studying axisymmetrically inflated biomembranes. IEEE Trans Biomed Eng 1995;42:442-50.
117. Hsu FP, Schwab C, Rigamonti D, Humphrey JD. Identification of response functions from axisymmetric membrane inflation tests: Implications for biomechanics. Int J Solids Struct 1994;31:3375-86.
118. Wang Z, Lakes RS, Chesler NC. Changes in conduit pulmonary arterial static and dynamic mechanical properties during severe hypoxic pulmonary hypertension. ASME 2012 Summer Bioengineering Conference, 2012.
119. Timoshenko SP. Strength of Materials. Part II. Advanced Theory and Problems. New York: D. Van Nostrand; 1956.
120. Deng SX, Tomioka J, Debbes JC, Fund YC. New experiments on shear modulus of elasticity of arteries. Am J Physiol Heart Circ Physiol 1994;266:H1-10.
121. Humphrey JD, Kang T, Sakarda P, Anjanappa M. Computer-aided vascular experimentation: A new electromenchanical test system. Ann Biomed Eng 1993;21:33-43.
122. Fung YC, Zweifach BW, Intaglietta M. Elastic environment of the capillary bed. Circ Res 1966;19:441-61.
123. Arbogast KB, Thibault KL, Pinheiro BS, Winey KI, Margulies SS. A high-frequency shear device for testing soft biological tissues. J Biomech 1997;30:757-9.
124. Dokos S, LeGrice IJ, Smaill BH, Kar J, Young AA. A triaxial-measurement shear-test device for soft biological tissues. J Biomech Eng 2000;122:471-8.
125. Huang W, Delgado-West D, Wu JT, Fung YC. Tissue remodeling of rat pulmonary artery in hypoxic breathing. II. Course of change of mechanical properties. Ann Biomed Eng 2001;29:552-62.
126. Holzapfel, GA, Ogden, RW. On planar biaxial tests for anisotropic nonlinearly elastic solids. A continuum mechanical framework. Math Mech Solids 2009;14:474-89.
127. Lu QJ, Ganesan K, Simionescu DT, Vyavahare NR. Novel porous aortic elastin and collagen scaffolds for tissue engineering. Biomaterials 2004;25:5227-37.
128. Sheridan WS, Duffy GP, Murphy BP. Mechanical characterization of a customized decellularized scaffold for vascular tissue engineering. J Mech Behav Biomed Mater 2012;8:58-70.
129. Williams C, Liao J, Joyce EM, Wang B, Leach JB, Sacks MS, et al. Altered structural and mechanical properties in decellularized rabbit carotid arteries. Acta Biomater 2009;5:993-1005.

Source of Support: This study is supported by National Institutes of Health (NIH) grants R01-HL086939 and R01-HL105598., **Conflict of Interest:** None declared.